# Experiments and analyses of a new type optical system for computed radiography

**Meng Zheng (郑 猛)[1], Qibo Feng (冯其波)[1*], Zhan Gao (高 瞻)[1], Shuangyun Shao (邵双运)[1], and Keqing Ding (丁克勤)[2]**

[1] *School of Science, Beijing Jiaotong University, Beijing 100044, China*

[2] *China Special Equipment Inspection and Research Center, Beijing 100013, China*

[*] *E-mail: qbfeng@bjtu.edu.cn*

Received April 14, 2010

A new high-performance laser scanning system is designed. In this system, a scanning arm consisting of a pentagonal prism and a scanning object lens is used to replace the traditional $F\theta$ lens, and a circular imaging plate transmission mechanism is specially designed in order to meet the requirement of the scanning arm. At the same time, the stimulation fluorescence can be obtained by the scanning arm. Some main factors that influence the spatial resolution and the performance of the laser scanner system are analyzed, and the analysis results are presented, which is helpful for further optimization design of the system. Experimental results indicate that the images obtained by the system have good visual effects and can meet the requirements of industrial inspection.

*OCIS codes:* 110.7440, 120.4570, 120.4820, 350.5500.

*doi: 10.3788/COL20100808.0800.*

Computed radiography (CR)[1−3] is an advanced digital imaging technology, which can replace the conventional $x$-ray screen-film with a reusable imaging plate (IP) coated with a photo-stimulating storage phosphor. Compared with the conventional films, the great advantages of IP are wider dynamic range, higher spatial resolution, larger detection area, higher detective efficiency, and reusability[4,5]. Therefore, it is widely used in many fields such as medical diagnosis, oil industry, natural gas, electricity engineering, and aviation in recent years. Laser scanner is a key component of CR system. Therefore, how to improve its collection efficiency and spatial resolution is always the focus in this research field.

Traditionally, in the laser scanning system of CR, a polygonal mirror is commonly used as a scanner, and an $F\theta$ lens is used to focus the laser beam[6,7], but it still has some limitations. For example, the polygonal mirror will generate scanning intermission, making the signal not be continuous; in addition, the $F\theta$ lens can make the whole system larger. In the existing products, the laser scanning system and the receiving system are usually separated[8,9], which makes the whole system complicated. To solve the above problems, a novel laser scanning system based on the scanning arm is designed. The scanning arm is composed of a pentagonal prism and a scanning object lens which is used to replace the $F\theta$ lens. A circular IP transport mechanism is designed to cooperate with the scanning arm. Meanwhile, the stimulated fluorescence can be received through the same scanning arm, which makes the whole system simple, compact, and exhibit better performance.

The laser scanning system is shown in Fig. 1. We employed an IP with the peak fluorescence wavelength of 390 nm and bandwidth of 40 nm. Because of this, a 638-nm laser was selected as the scanning source. As shown in Fig. 1, the scanning arm, which is composed of a pentagonal prism and a scanning objective lens, can be rotated by a motor around the axis that is also the optical axis of the emitting optical system including the laser and laser beam expander. The IP is placed on the circular plane by the transport mechanism, and this circular plane is also the focus plane of the scanning objective lens, thus ensuring that the laser beam can always scan the IP perpendicularly and that the spot size of the laser beam on the IP is the smallest and unchanged. Meanwhile, the fluorescence from the IP can be collected by a photomultiplier tube (PMT) through the same scanning arm.

The whole work procedure of the laser scanning is as follows. The laser beam, which is collimated and expanded by the beam expander, passes through the beam splitter, and it is reflected by the pentagonal prism. The reflected laser beam is then focused on the IP by the scanning objective lens. The fluorescence from the focus point on the IP becomes a parallel beam by the scanning objective lens; it is reflected by the pentagonal prism and the beam splitter and is focused into the PMT by a condenser lens. The stray light can be removed by using a filter. The fluorescence signal collected by the PMT

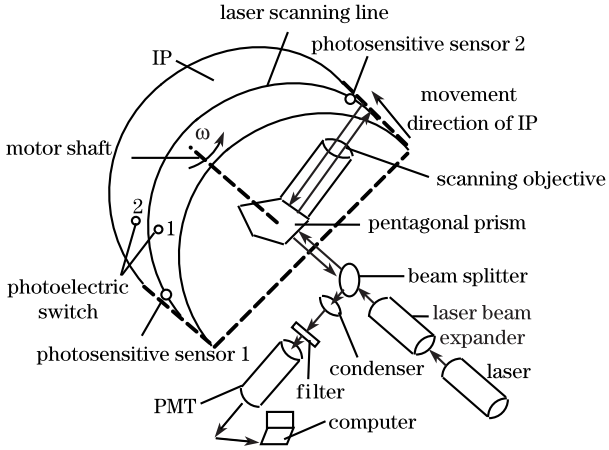


Fig. 1. Configuration of laser scanning optical system.

 

is sent to the computer after analog-digital conversion and a digital image of fluorescence from the IP can be formed when the scanning arm rotates around the axis and the IP is driven to move longitudinally. Here, a special beam splitter that can almost totally transmit the laser beam with the wavelength of 638 nm and almost totally reflect the florescence with the wavelength of 390 nm was adopted in order to enhance the collection efficiency of the florescence.

As shown in Fig. 1, four sensors including two photoelectric switches and two photosensitive sensors are used to realize the synchronization and controlling of scanning, longitudinal movement of the IP, and signal collection. Two photoelectric switches are longitudinally located on both sides of the laser scanning line, and their signals are used to detect in and out of the IP. Two photosensitive sensors, which are triggered by the scanning laser beam, are located on the laser scanning line. When the scanning laser beam passes through the photosensitive sensor 1, the signal from the sensor 1 triggers the controlling circuit, the fluorescence signal is to be collected, and the imaging plate does not move; when the scanning laser beam passes through the photosensitive sensor 2, the circuit controls the IP to move a step longitudinally and stops the fluorescence signal collection. In this way, the data are obtained in the positive half cycle of the rotating scanning arm and the IP moves one step in the negative half cycle of rotating scanning arm.

Some experiments were done in order to find the main factors that influence the spatial resolution and collection efficiency of fluorescence in the system. The experimental results with two different laser spot sizes are shown in Fig. 2. In this experiment, 21 lead wires, whose diameters are decreased in sequence, are exposed on the IP and the fluorescence intensity values are obtained with this system. The curves 1 and 2 show the scanning results with 0.5- and 0.8-mm spot size, respectively. The downward peaks show the positions of the scanned lead wires. The 16 wire can be clearly distinguished in curve 1, while only the 13 wire can be discerned in curve 2. Therefore, the smaller spot size of laser beam is, the higher spatial resolution of the system is.

The experimental results indicating the relationship between the laser beam incident angles and fluorescence collection efficiency is shown in Fig. 3. It can be seen that the collected fluorescence intensity is gradually reduced when the incident angle is increased, and it achieves the maximum when the incident beam is perpendicular to the IP.

In the system, the greatest impact on the system spatial resolution is the assembly error of mechanical structure,

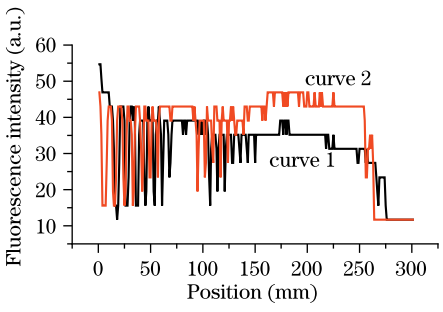


Fig. 2. Scanning comparison with two laser spot sizes.

especially the IP position error. Now we carry out deep analysis on this error. Scanning arm is a key component, whose mechanical structure is shown in Fig. 4. Because of the installation errors of the laser or the scanning arm, the incident beam may not be perpendicular to the surface of the pentagonal prism, thus making the exit beam be not perpendicular to the IP, as shown in Fig. 5.

The pentagonal prism is equivalent to the parallel glass panel, and the propagation of off-axis Gaussian beams through the $ABCD$ optical system is shown in Fig.6. The intensity distribution and the influence of an off-axis Gaussian beam on the spatial resolution can be analyzed by numerical calculation[10−12].

The input reference plane is located at the position of the waist of the incident Gaussian beam, and the output reference plane can be located at any position after the scanning objective lens. To simplify the analysis, only one-dimensional situation is considered. The optical field distribution of the incident Gaussian beam in the input reference plane is

$$E_0(y_0, 0) = \exp\left[-\frac{(y_0 - \Delta y)^2 \cos^2\theta}{\omega_0^2}\right], \quad (1)$$

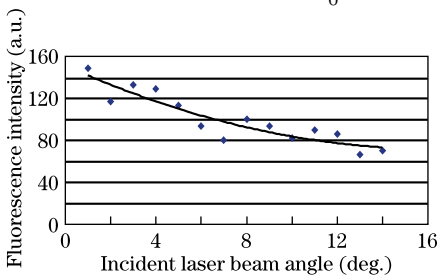


Fig. 3. Relationship between incident angle and fluorescence intensity.

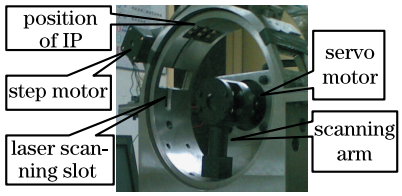


Fig. 4. Mechanical structure of the scanning arm.

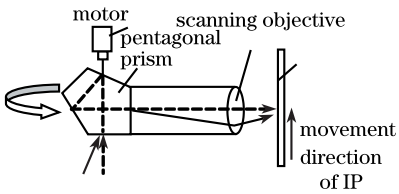


Fig. 5. Sketch of incident light out of direction vertical to IP.

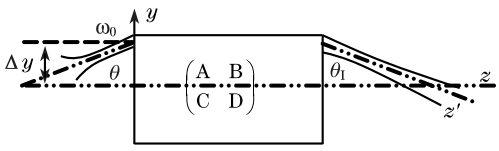


Fig. 6. Sketch of off-axis beam passing through the optical system.

where $y_0$ is the coordinate value of the input reference plane, $\Delta y$ is the distance between the axis of the incident Gaussian beam and the axis of the optical system in the input reference plane, $\omega_0$ is the Gaussian beam waist radius.

When the Gaussian beams pass through the $ABCD$ optical system, the optical field distribution of the Gaussian beam in the output reference plane can be calculated by Collins formula as

$$E_1(y_1,z) = \sqrt{\frac{\mathrm{i}k}{2\pi B}} \int_{-\infty}^{+\infty} E_0(y_0,0) \cdot \exp\left[-\frac{\mathrm{i}k}{2B}(Ay_0^2 - 2y_0y_1 + Dy_1^2)\right] \mathrm{d}y_0, \quad (2)$$

where $k$ is the wave number, $A, B$, and $D$ are parameters of the $ABCD$ matrix.

Substituting Eq. (1) into Eq. (2) and using

$$\int_{-\infty}^{+\infty} \exp(-p^2x^2 \pm qx)dx = \frac{\sqrt{\pi}}{p}\exp\left(\frac{q^2}{4p^2}\right), p > 0, \quad (3)$$

Eq. (2) can be written as

$$E_1(y_1,z) = \sqrt{\frac{ik}{2\pi B}} \cdot \exp\left(-\frac{\mathrm{i}kDy_1^2}{2B}\right) \cdot p\left(-\frac{\Delta y^2\cos^2\theta}{\omega_0^2}\right) \cdot \frac{\sqrt{\pi}}{p} \cdot \exp\left[-\frac{k^2(y_1-q)^2}{4B^2p^2}\right], \quad (4)$$

where $q = \frac{2\mathrm{i}\Delta yB\cos^2\theta}{k\omega_0^2}$, $p^2 = \frac{\cos^2\theta}{\omega_0^2} + \frac{\mathrm{i}kA}{2B}$.

The intensity distribution of the Gaussian beam in the output reference plane is

$$I_1(y_1,z) = E_1(y_1,z)\cdot E_1^*(y_1,z), \quad (5)$$

where $E_1(y_1,z)$ and $E_1^*(y_1,z)$ are conjugated. Substituting Eq. (4) into Eq. (5), we get

$$I_1(y_1,z) = \sqrt{\frac{k^2}{4\pi^2B^2}} \cdot \exp\left(-\frac{2\Delta y^2\cos^2\theta}{\omega_0^2}\right) \cdot \frac{\pi}{\sqrt{\frac{\cos^4\theta}{\omega_0^4} + \frac{k^2A^2}{4B^2}}} \cdot \exp\left(-\frac{k^2}{4B^2}\cdot\frac{q_1}{p_1}\right), \quad (6)$$

where $p_1 = \frac{\cos^4\theta}{\omega_0^2} + \left(\frac{kA\omega_0}{2B}\right)^2$, $q_1 = 2y_1^2\cos^2\theta - \frac{8\Delta y^2B^2\cos^6\theta}{k^2\omega_0^4} - 4y_1\Delta yA\cos^2\theta$.

The incident beam waist is located in front of the incident plane of the pentagonal prism, and the input reference plane is located in the plane of the Gaussian beam waist. When the output reference plane is located in the focal plane of the scanning objective (IP is located in this position, and the scanning objective is a doublet lens), the parameters of the $ABCD$ matrix from the incident beam waist to the focal plane of the doublet lens can be obtained. Substituting these parameters into Eq. (6), the intensity distribution of output reference plane can be acquired.

When $\Delta y = 2$ mm and $\theta = 1°$, the intensity distributions when the laser point locations are 2 mm before, in, and 3 mm after the focal plane are shown in Fig. 7. It can be seen that there will be the largest fluorescence intensity and the smallest spot diameter if the laser beam is focused on the focal plane. When there exists the IP position error, namely, the IP and the focal plane of doublet lens are in different planes when scanned by Gaussian beams, light intensity decreases and the change of spot diameter is larger, leading to a greater impact on the spatial resolution of the system.

When the incident angle becomes larger, the collected fluorescence intensity is decreased. So, it is very important to keep the laser beam being imaged on the focus plane and being perpendicular to the IP.

At present, the spatial resolution is generally no less than 3 lp/mm in industrial radiographic inspection. Through a standard test, it was found that the spatial resolution of our system was 7 lp/mm, which could meet the requirements of the national standard of industrial radiographic inspection in China.

A specimen of pipe weld was selected in the experiment. The diameter of the pipe was 160 mm and the thickness was 8 mm. The IP was placed inside the pipe, as shown in Fig. 8.

The X-ray tube voltage used in the experiment had a voltage of 120 kV and a current of 4 mA; the focal length was 700 mm; and the exposure time of IP was 40 s. The image obtained by our system is shown in Fig. 9. The small weld defects can be clearly displayed without any image processing.

In conclusion, a novel laser scanning system for CR is presented, and some main factors which influence the spatial resolution and the collection efficiency are analyzed. It is found that the smaller the spot size is, the higher the spatial resolution is, and the larger the incident angle is, the lower the collectionl efficiency is. The assembly position relationship of the scanning arm with

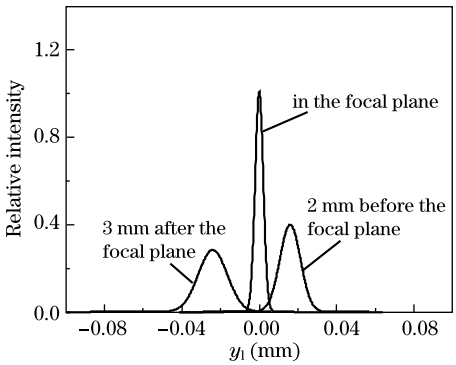


Fig. 7. Intensity distributions for different laser point locations.

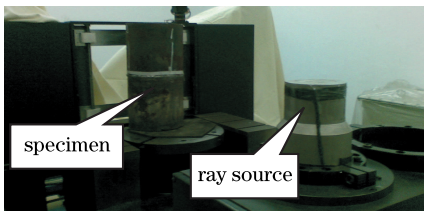


Fig. 8. Experiment arrangement of radiography.

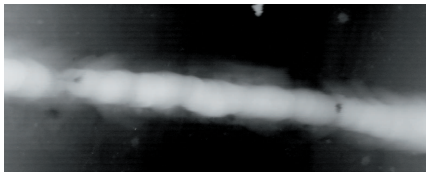

Fig. 9. Original image of scanning.

the IP has significant influence on the spatial resolution and collection efficiency.

This work was supported by the National Scientific and Technical Supporting Program of China under Grant NO. 2006BAK02B01.

## References

1. A. R. Cowen, A. G. Davies, and S. M. Kengyelics, Clinical Radiology **62,** 1132 (2007).
2. K. Sakasai, M. Katagiri, M. Kishimoto, T. Nakamura, K. Toh, H. Takahashi, and M. Nakazawa, in *Proceedings of IEEE Conference on Nuclear Science* 673 (2000).
3. F.-Y. Hou, Opt. Prec. Eng. (in Chinese) **6,** (5) 96 (1998).
4. H. Nanto, A. Nishimura, M. Kuroda, Y. Takei, Y. Nakano, T. Shoji, T. Yanagita, and S. Kasai, Nuclear Instrum. Methods Phys. Res. A **580,** 278 (2007).
5. H. Nanto, T. Sato, T. Shinkawa, M. Miyazaki, A. Imai, E. Kusano, A. Kinbara, S. Nasu, and Y. Douguchi, Proc. SPIE **3336,** 564 (1998).
6. J. Zhang, X. Feng, L. Huang, C. Yang, and X. Zhang, Opt. Prec. Eng. (in Chinese) **16,** 202 (2008).
7. M. B. Brandt and M. R. Flynn, "Light collector having optically coated acrylic substrate" US patent 5,541,421 (July 30, 1996).
8. R. Schaetzing, R. Fasbender, and P. Kersten, Proc. SPIE **4682,** 511 (2002).
9. M. Brandt, Proc. SPIE **1896,** 288 (1993).
10. A.-A. R. Al-Rashed and B. E. A. Saleh, Appl. Opt. **34,** 6819 (1995).
11. B. Chen, J. Pu, Z. Zhang, and X. Wang, Acta Opt. Sin. (in Chinese) **29,** 1664 (2009).
12. Y. Zhao, H. Sun, F. Song, and D. Dai, Acta Opt. Sin. (in Chinese) **29,** 2552 (2009).